Modeling pO_2 Distributions in the Bone Marrow Hematopoietic Compartment. II. Modified Kroghian Models

Dominic C. Chow, Larissa A. Wenning, William M. Miller, and E. Terry Papoutsakis
Department of Chemical Engineering, Northwestern University, Evanston, Illinois 60208-3120 USA

ABSTRACT Hematopoietic cells of various lineages are organized in distinct cellular architectures in the bone marrow hematopoietic compartment (BMHC). The homogeneous Kroghian model, which deals only with a single cell type, may not be sufficient to accurately describe oxygen transfer in the BMHC. Thus, for cellular architectures of physiological significance, more complex biophysical-transport models were considered and compared against simulations using the homogeneous Kroghian model. The effects of the heterogeneity of model parameters on the oxygen tension (pO_2) distribution were examined using the multilayer Kroghian model. We have also developed two-dimensional Kroghian models to simulate several cellular architectures in which a cell cluster (erythroid cluster) or an individual cell (megakaryocyte or adipocyte) is located in the BMHC predominantly occupied by mature granulocytes. pO_2 distributions in colony-type cellular arrangements (erythroblastic islets, granulopoietic loci, and lymphocytic nodules) in the BMHC were also evaluated by modifying the multilayer Kroghian model. The simulated results indicate that most hematopoietic progenitors experience low pO_2 values, which agrees with the finding that low pO_2 promotes the expansion of various hematopoietic progenitors. These results suggest that the most primitive stem cells, which are located even further away from BM sinuses, are likely located in a very low pO_2 environment.

NOMENCLATURE

i = index number
j = number of cell layers
K = oxygen permeability (mol/cm/s/mmHg)
K_i = oxygen permeability of the ith layer (mol/cm/s/mmHg)
N = total number of cell layers
N_{tot} = total number of finite elements in the tissue cylinder
P = oxygen partial pressure (tension) (mm Hg)
P_S = saturation oxygen tension (mm Hg)
P^* = reduced oxygen tension
P^*_{R2} = reduced oxygen tension at the outer boundary of the tissue cylinder
$P_{i,j}$ = oxygen partial pressure at point (i, j) (mm Hg)
Q = volumetric oxygen uptake rate (mol/cm^3/s)
Q_i = volumetric oxygen uptake rate of the ith layer (mol/cm^3/s)
r = distance from the center of the tissue cylinder (μm)
r^* = reduced distance from the center of the tissue cylinder
R_i = distance from the center of the tissue cylinder to the ith interface (μm)

Coefficients

a_i = coefficient in Eq. 11
$a_{i,j}$ = coefficient in Eq. A5
A = N_{tot} by N_{tot} matrix containing all the coefficients of Eq. A12
b_i = coefficient in Eq. 11
$b_{i,j}$ = coefficient in Eq. A5
B = N_{tot} by 1 matrix containing the coefficients of Eq. A12
$c_{i,j}$ = coefficient in Eq. A5
$d_{i,j}$ = coefficient in Eq. A5
X = N_{tot} by 1 matrix containing all oxygen tensions on the mesh

Greek symbols

β_i = reduced distance from the center of the tissue cylinder to the ith interface
$\chi_{i,j}$ = ratio of effective permeability of the ith layer to that of the jth layer
ϕ_i = Thiele modulus of the ith layer
θ = angle (degree)

INTRODUCTION

In the first part of this two-part series we presented estimates for various model parameters and developed a mathematical framework (homogeneous Kroghian model) to evaluate oxygen tension (pO_2) distributions in the bone marrow hematopoietic compartment (BMHC), assuming that the extravascular tissue is composed of only one cell type. However, compared to muscle tissue, for which the Kroghian model was developed, the BMHC contains unique and complex cellular architectures made up of multiple cell

Received for publication 8 December 2000 and in final form 24 April 2001.

Address reprint requests to E. Terry Papoutsakis, Dept. Chemical Engineering, Northwestern University, 2145 Sheridan Road E136, Evanston, IL 60208-3120. Tel: 847-491-7398; Fax: 847-491-3728; E-mail: e-paps@nwu.edu.

Dr. Wenning's present address: Department of Drug Metabolism, Merck Research Laboratories, West Point, PA 19486.

0006-3495/01/08/685/12 $2.00

types, which exist in layers and clustering arrangements (Adler, 1984; Lichtman, 1984; Tavassoli and Yoffey, 1983; Weiss, 1991; Wickramasinghe, 1975). This raises the question of how well the simple Kroghian model approximates these complex physiological features.

Since Krogh's original publication, many efforts have been reported toward improving the predictions of the Kroghian model by incorporating various physiological features and cellular characteristics (Fletcher, 1980; Hoofd and Kreuzer, 1979; Popel, 1982; Popel et al., 1986). Somewhat surprisingly, the calculated pO_2 distributions in muscle tissue were not significantly affected by model modifications to account for facilitated diffusion due to the presence of hemoglobin and myoglobin (Federspiel, 1986; Federspiel and Popel, 1986; Fletcher, 1980; Hoofd et al., 1994), asymmetric diffusion (Rakusan et al., 1984), or oxygen-dependent oxygen consumption (Fletcher, 1978; Hoofd et al., 1987). Substantial model modifications are, however, necessary for tissues with spatial heterogeneity and non-Kroghian geometry (not cylindrically symmetric) (Grossmann, 1982; Ivanov et al., 1979; Reneau et al., 1967).

The challenges in mathematically modeling pO_2 distributions in the BMHC result from the complexity of cellular architectures in the BMHC. Hematopoietic cells present in the BMHC belong to different cell lineages and stages of differentiation and include, among others, totipotent and pluripotent hematopoietic stem cells, colony-forming cells (CFC), and differentiated lineage-committed cells (granulocytes, monocytes, lymphocytes, megakaryocytes, and erythrocytes). Thus, hematopoietic cells of different lineages and stages of differentiation exist in the proximity of each other and of stromal cells such as adipocytes, and are unlikely to be arranged in the cylindrically symmetric geometry that is assumed in the original Kroghian model. Also, hematopoietic cells of different lineages often follow distinct patterns of cellular arrangements (as discussed in the introduction of the first part of the present two-part study). For example, mature erythrocytes and megakaryocytes reside in the regions close to the sinus, while erythroid and granulocytic progenitors are found away from the sinus (Weiss, 1991). Therefore, specific cellular architectures should be considered separately.

In light of these physiological considerations we have modified the homogeneous Kroghian model to evaluate the effects of heterogeneity in cellular properties on pO_2 distribution in the BMHC by dividing the extravascular tissue into multiple cell layers with different metabolic and transport characteristics (multilayer model). We have also developed a two-dimensional model to describe complicated cellular architectures that more closely approximate physiologically significant cellular configurations in the hematopoietic tissue. Finally, we have modified the multilayer Kroghian model to simulate the pO_2 distributions in colony-type cellular arrangements, such as in erythroblastic islets, granulocytic loci, and lymphocytic nodules. Simulation results from these models were compared with those estimated in the homogeneous Kroghian model.

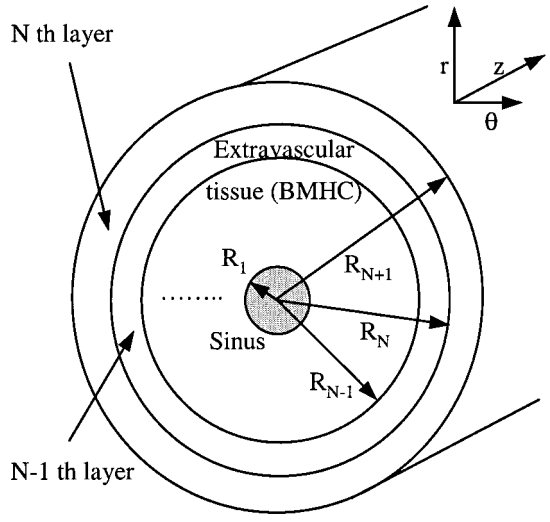

FIGURE 1 Graphical representation of the multilayer Kroghian model.

METHODS

Multilayer Kroghian model

In the multilayer model the extravascular hematopoietic tissue is divided into separate cell layers surrounding a sinus (Fig. 1). Based on the same assumptions as the original Krogh model, oxygen transfer and consumption for each layer can be mathematically described as follows.

$$\frac{1}{r}\left[\frac{d}{dr}\left(r\frac{dP_i}{dr}\right)\right] = \frac{Q_i(P_i)}{K_i} \quad \text{for} \quad R_i < r \le R_{i+1} \tag{1}$$

where P_i is the pO_2, K_i is the oxygen permeability, and $Q_i(P_i)$ is the volumetric oxygen uptake rate of the ith cell layer, respectively. R_i and R_{i+1} are the distance from the center of the tissue cylinder to the ith and $(i + 1)$th interface, respectively. We assume that pO_2 at the sinus wall (R_1) equals the saturation oxygen tension (P_S) and that the oxygen flux is zero when it reaches the boundary of the tissue cylinder (R_{N+1}). There is continuity of the oxygen flux and pO_2 at the interface between two layers. Thus, the boundary conditions are as follows.

$$P_1 = P_S \; at \; r = R_1 \text{ (at the sinus wall)} \tag{2}$$

$$-K_i\frac{dP_i}{dr} = -K_{i+1}\frac{dP_{i+1}}{dr} \quad \text{at} \quad r = R_{i+1}$$

$$\text{(at the } (i + 1)\text{th interface)} \tag{3}$$

$$P_i = P_{i+1} \quad at \quad r = R_{i+1}$$

$$\text{(at the } (i + 1)\text{th interface)} \tag{4}$$

$$\frac{dP_N}{dr} = 0 \quad \text{at} \quad r = R_{N+1}$$

$$\text{(at the rim of the tissue cylinder)} \tag{5}$$

where P_1 and P_N are the oxygen tensions on the first and Nth cell layer, respectively. Using P_S and R_{N+1} as the characteristic oxygen tension and characteristic length, and multiplying both sides of Eq. 1 by R_{N+1}^2/P_S, the dimensionless boundary value problem becomes

$$\frac{1}{r^*}\frac{d}{dr^*}\left(r^*\frac{dP_i^*}{dr^*}\right) = \frac{Q_i(P_i)}{K_i}\frac{R_{N+1}^2}{P_S} = \phi_i^2 \tag{6}$$

$$P_1^* = 1 \quad \text{at} \quad r^* = \beta_1 \text{ (at the sinus wall)} \tag{7}$$

$$\chi_{i,i+1}\frac{dP_i^*}{dr^*} = \frac{dP_{i+1}^*}{dr^*} \quad \text{at} \quad r^* = \beta_{i+1}$$

$$\text{(at the } (i+1)\text{th interface)} \tag{8}$$

$$P_i^* = P_{i+1}^* \quad \text{at} \quad r^* = \beta_{i+1}$$

$$\text{(at the } (i+1)\text{th interface)} \tag{9}$$

$$\frac{dP_N^*}{dr^*} = 0 \quad \text{at} \quad r^* = 1$$

$$\text{(at the rim of the tissue cylinder)} \tag{10}$$

where ϕ_i is the Thiele modulus of the ith layer, β_i is the dimensionless distance from the center of the tissue cylinder to the ith interface, and $\chi_{i,i+1}$ is the ratio of K_i to K_{i+1}. The solution to this problem describes the reduced oxygen tension P_i^* at the ith cell layer at a distance r^* from the center of the tissue cylinder (Chow, 2000):

$$P_i^*(r^*) = 1 + \sum_{\substack{j=1 \\ i>j}}^{i-1}\left[a_j ln\left(\frac{\beta_j}{\beta_{j+1}}\right) + b_j(\beta_{j+1}^2 - \beta_j^2)\right] + a_i ln\left(\frac{\beta_i}{r^*}\right) + b_i(r^{*2} - \beta_i^2) \tag{11}$$

where

$$a_j = \frac{1}{2}\sum_{m=j}^{N}\beta_{m+1}^2(\chi_{m,j}\cdot\phi_m^2 - \chi_{m+1,j}\cdot\phi_{m+1}^2) \tag{12}$$

$$b_j = \frac{1}{4}\phi_j^2 \tag{13}$$

$$\phi_j = R_{N+1}\sqrt{\frac{Q_j}{K_j\cdot P_S}} \tag{14}$$

$$\chi_{m,j} = \frac{K_m}{K_j} \tag{15}$$

where Q_j is a constant for each layer j. Note that $\phi_{N+1} = 0$ and $\beta_{N+1} = 1$. Solutions for the cases of the one-, two-, and three-layer Kroghian model are shown in Table 1.

TABLE 1 Summary of dimensionless solutions for the one-, two-, and three-layer dimensionless multilayer models

$P_i^* - 1$	Constants		
1st Layer ($i = 1$)	2nd Layer ($i = 2$)	3rd Layer ($i = 3$)	C_1	C_2	C_3
1-Layer model ($N = 1$) $C_1\cdot\ln\frac{\beta_1}{r^*} + \frac{\phi_1^2}{4}(r^{*2} - \beta_1^2)$	—	—	$\frac{1}{2}\phi_1^2$	—	—
2-Layer model ($N = 2$) $C_1\cdot\ln\frac{\beta_1}{r^*} + \frac{\phi_1^2}{4}(r^{*2} - \beta_1^2)$	$C_1\cdot\ln\frac{\beta_1}{\beta_2} + \frac{\phi_1^2}{4}(\beta_2^2 - \beta_1^2) + C_2\cdot\ln\frac{\beta_2}{r^*} + \frac{\phi_2^2}{4}(r^{*2} - \beta_2^2)$	—	$\frac{\beta_2^2}{2}(\phi_1^2 - \chi_{2,1}\cdot\phi_2^2) + \chi_{2,1}\cdot C_2$	$\frac{1}{2}\phi_2^2$	—
3-Layer model ($N = 3$) $C_1\cdot\ln\frac{\beta_1}{r^*} + \frac{\phi_1^2}{4}(r^{*2} - \beta_1^2)$	$C_1\cdot\ln\frac{\beta_1}{\beta_2} + \frac{\phi_1^2}{4}(\beta_2^2 - \beta_1^2) + C_2\cdot\ln\frac{\beta_2}{r^*} + \frac{\phi_2^2}{4}(r^{*2} - \beta_2^2)$	$C_1\cdot\ln\frac{\beta_1}{\beta_2} + \frac{\phi_1^2}{4}(\beta_2^2 - \beta_1^2) + C_2\cdot\ln\frac{\beta_2}{\beta_3} + \frac{\phi_2^2}{4}(\beta_3^2 - \beta_2^2) + C_3\cdot\ln\frac{\beta_3}{r^*} + \frac{\phi_3^2}{4}(r^{*2} - \beta_3^2)$	$\frac{\beta_2^2}{2}(\phi_1^2 - \chi_{2,1}\cdot\phi_2^2) + \chi_{2,1}\cdot C_2$	$\frac{\beta_3^2}{2}(\phi_2^2 - \chi_{3,2}\cdot\phi_3^2) + \chi_{3,2}\cdot C_3$	$\frac{1}{2}\phi_3^2$

Two-dimensional Kroghian model

An additional spatial dimension is considered to describe cellular architectures in which cells are arranged as a cluster, and the model formulation of the two-dimensional Kroghian model is depicted in Fig. 2. A similar model framework can be used to simulate the pO_2 distributions of a cellular

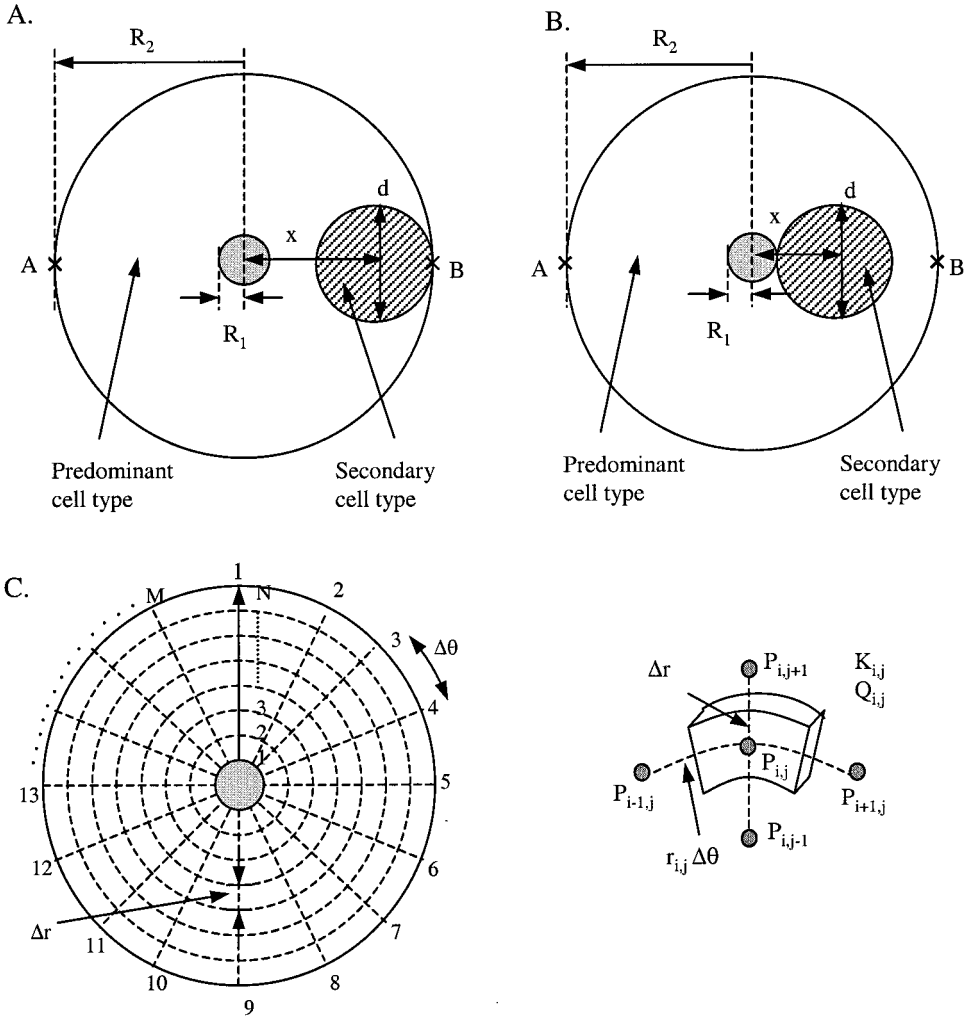

FIGURE 2 Graphical representation of cellular architectures used in the two-dimensional Kroghian model. (*A*) The secondary cell type is located far away from the sinus (far position); (*B*) the secondary cell type is located next to the sinus (close position); (*C*) finite elements of the tissue cylinder.

arrangement with hematopoietic cells that are substantially larger than other hematopoietic cells (for example, megakaryocytes or adipocytes) because they closely resemble the presence of a cell cluster in the tissue cylinder. Granulocytes are the predominant cell type in the BMHC (Chow et al., 2001), and thus are chosen to occupy most of the tissue cylinder. Other hematopoietic cell types such as megakaryocytes, erythrocytes, and adipocytes are placed as a cell cluster at any desired location in the extravascular tissue cylinder. We term these cells as secondary cell types because the volume that they occupy is relatively smaller than that of granulocytes. The predominant and secondary cell types have distinct cellular properties (as described by parameters Q and K). The diameters of the sinus (R_1) and the tissue cylinder (R_{N+1}) in all models are maintained the same so that simulation results (pO_2 values and gradients) can be compared directly. An individual hematopoietic cell or a cell cluster of diameter d is placed next to the boundary of the tissue cylinder (far position) or the sinus (close position) to evaluate differences on pO_2 distribution (Fig. 2, *A* and *B*). The distance between the centers of the tissue cylinder and the cell cluster is denoted by x.

Using the characteristic oxygen tension (P_S) and characteristic length (R_{N+1}), the two-dimensional model is described in the following boundary-value problem (in its dimensionless form):

$$\frac{1}{r^*}\frac{\partial}{\partial r^*}\left(r^*\frac{\partial P_1^*}{\partial r^*}\right)+\frac{1}{r^{*2}}\frac{\partial^2 P_1^*}{\partial \theta^2}=\frac{Q_1}{K_1}\frac{R_{N+1}^2}{P_S}$$
$$=\phi_1^2 \text{ (for the predominant cell type)} \quad (16)$$

$$\frac{1}{r^*}\frac{\partial}{\partial r^*}\left(r^*\frac{\partial P_2^*}{\partial r^*}\right)+\frac{1}{r^{*2}}\frac{\partial^2 P_2^*}{\partial \theta^2}=\frac{Q_2}{K_2}\frac{R_{N+1}^2}{P_S}$$
$$=\phi_2^2 \text{ (for the secondary cell type)} \quad (17)$$

where the Thiele moduli in the regions occupied by the predominant and secondary cell types are assumed to be constant, and are denoted by ϕ_1 and ϕ_2, respectively. The first two boundary conditions used in the two-dimensional Kroghian model are similar to those in the homogeneous Kroghian model. The oxygen tension at the sinus wall equals the saturation oxygen tension, and the oxygen flux is assumed to be zero at the rim of the tissue cylinder.

$$P_1^*(r^*, \theta)=1 \quad \text{at} \quad r^*=\beta_1$$

(at the sinus wall) (18)

$$\frac{dP_1^*(r^*, \theta)}{dr^*} = 0 \quad \text{at} \quad r^* = 1$$

(at the rim of the tissue cylinder) (19)

The other two boundary conditions regarding the continuity of oxygen tension and oxygen flux at the interface between the regions occupied by the predominant and secondary cell types are as follows:

$$\chi_{1,2}\frac{dP_1^*(r^*, \theta)}{dr^*} = \frac{dP_2^*(r^*, \theta)}{dr^*} \text{ (at the interface)} \quad (20)$$

$$P_1^*(r^*, \theta) = P_2^*(r^*, \theta) \text{ (at the interface)} \quad (21)$$

where $\chi_{1,2}$ is the ratio of the oxygen permeability coefficient of the predominant cell type to that of secondary cell type. $P_1^*(r^*, \theta)$ and $P_2^*(r^*, \theta)$ are the dimensionless oxygen tensions in the regions occupied by the predominant and secondary cells, respectively. The location of the interface (i.e., the values of r^* and θ) depends on the diameter of the secondary cell type ($\delta = d/R_{N+1}$) and the distance between the centers of the tissue cylinder and cell cluster ($\xi = x/R_{N+1}$). The solution of this class of boundary value problems was obtained using the finite difference method (FDM) (Na, 1979), in which an overall pO_2 profile is generated by a collection of finite elements representing average oxygen tensions in their proximity (Fig. 2 *C*). The tissue cylinder in the two-dimensional model is divided into $M \times N$ elements with dimensions Δr by $r_{i,j}\Delta\theta$. The values of cellular properties of these elements depend on their location on the tissue cylinder; in our model they can be the properties of either the predominant or secondary cell type. Detailed calculations for the oxygen tension of each element are shown in the Appendix.

Oxygen tension distribution in colony-type cellular arrangements

In addition to the cellular configurations previously described, several cellular architectures of the BMHC that are not well described by the mathematical framework in the original Kroghian model are commonly reported in the literature. Hematopoietic cells frequently form multilayer clusters, which are surrounded by a network of sinuses in the BMHC. For example, erythroblastic islets usually consist of one or two macrophages surrounded by multiple layers of erythroid progenitors and mature erythrocytes. The multilayer Kroghian model with suitable modifications can be used to simulate this type of cellular architecture. This mathematical formulation can also be applied to other cell clusters (granulocytic loci or lymphocytic nodules) or individual cells (megakaryocytes or adipocytes) located in a well-vascularized region in the BMHC.

Using a similar model framework as described in Fig. 1, regions in the tissue cylinder can be reassigned with different physiological features in the well-vascularized hematopoietic tissue (Fig. 3). First, the sinus radius (R_1) in the multilayer Kroghian model is assumed to be zero and the oxygen flux at the center of the tissue cylinder is assumed to be zero. The boundary conditions for the interfaces described in the original multilayer Kroghian model still hold for this model. The network of sinuses around the hematopoietic tissue can be modeled as a layer of vasculature that completely surrounds the hematopoietic cells. For simplicity, the saturation oxygen tension at the interface between the sinus and hematopoietic cells is assumed to be constant and equal to P_S. For the cellular architecture described in Fig. 3, the oxygen profile of each layer can be obtained by solving the following set of boundary value problems.

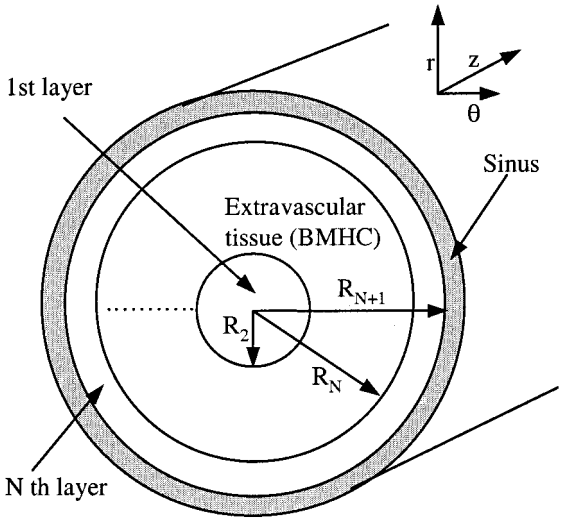

FIGURE 3 Graphical representation of a region of hematopoietic tissue (erythroblastic islet) surrounded by a network of sinuses.

$$\frac{1}{r}\frac{dP_i}{dr} + \frac{d^2P_i}{dr^2} = \frac{Q_i}{K_i} \text{ (for the } i\text{th layer)} \quad (22)$$

$$\frac{dP_1}{dr} = 0 \quad \text{at} \quad r = R_1 = 0$$

(at the center of the tissue cylinder) (23)

$$P_i = P_{i+1} \quad at \quad r = R_{i+1}$$

(at the ith interface) (24)

$$-K_i\frac{dP_i}{dr} = -K_{i+1}\frac{dP_{i+1}}{dr} \quad \text{at} \quad r = R_{i+1}$$

(at the ith interface) (25)

$$P_N = P_S \quad at \quad r = R_{N+1}$$

(at the rim of the vasculature) (26)

Using P_S and R_{N+1} as the characteristic oxygen tension and characteristic length, and multiplying both sides of Eq. 22 by R_{N+1}^2/P_S, the set of dimensionless boundary value problems becomes

$$\frac{1}{r^*}\frac{dP_i^*}{dr^*} + \frac{d^2P_i^*}{dr^{*2}} = \frac{Q_i}{K_i}\frac{R_{N+1}^2}{P_S} = \phi_i^2 \quad (27)$$

$$\frac{dP_1^*}{dr^*} = 0 \quad \text{at} \quad r^* = \beta_1 = 0$$

(at the center of the tissue cylinder) (28)

$$P_i^* = P_{i+1}^* \quad \text{at} \quad r^* = \beta_{i+1}$$

(at the ith interface) (29)

$$\chi_{i,i+1}\frac{dP_i^*}{dr^*} = \frac{dP_{i+1}^*}{dr^*} \quad \text{at} \quad r^* = \beta_{i+1}$$

(at the ith interface) (30)

$$P_N^* = 1 \quad \text{at} \quad r^* = 1$$

(at the rim of the vasculature) (31)

Model parameters are defined in the same manner as in the multilayer model. The solutions for each cell layer in one-, two-, and three-layer dimensionless models are summarized in Table 2.

RESULTS

Multilayer Kroghian models

Among all possible cellular architectures in the BMHC, we are interested in those of physiological significance. Based on the differential counts reported in the literature (Table 2 in Chow et al., 2001), granulocytes are the most abundant cell type in the BM. The oxygen uptake rate (q_{O2}) of hematopoietic cells, which varies the most among all biophysical parameters estimated from the literature, is expected to strongly affect the model simulation results. Experimental results from our group indicate that the oxygen metabolism of granulocytic progenitors (G_P) and mature granulocytes (G_M) are substantially different (q_{O2} values of G_P and G_M are 6.49×10^{-13} and 2.2×10^{-14} mol/cell/h, respectively) (Collins et al., 1998). Therefore, we examined pO_2 distribution in a tissue cylinder containing G_P and G_M, assuming that all cellular properties except for q_{O2} are the same.

Results reported in the companion paper (Chow et al., 2001) indicated that oxygen depletion occurs in a tissue cylinder containing three layers of G_P. To demonstrate the effects of the heterogeneity of cellular properties, we considered tissue cylinders containing three cell layers of granulocytes with an increasing number of layers of G_P placed at different locations (the rest of the tissue was occupied by G_M) (Fig. 4). Oxygen availability is reduced as the number of G_P layers is increased. Oxygen is depleted when the two outermost cell layers are occupied by G_P. Variations in pO_2 are greater when the metabolically active G_P are located away from a sinus, which physiologically is the most likely configuration (Chow et al., 2001). Among the cellular configurations shown in Fig. 4, those with G_P close to the sinus ($G_PG_MG_M$ and $G_PG_PG_M$) are less likely to be found in the BMHC.

Two-dimensional Kroghian models

Based on the simulation results from the homogeneous Kroghian model (Fig. 2 of Chow et al., 2001) and the predominance of granulocytic cells in the BMHC, cellular configurations with mature granulocytes in combination with other cell types were constructed to examine how

TABLE 2 Summary of analytical solutions for the one-, two-, and three-layer models with modified boundary conditions

	$P_i^* - 1$			Constants		
	1st Layer ($i = 1$)	2nd Layer ($i = 2$)	3rd Layer ($i = 3$)	C_4	C_5
1-Layer model ($N = 1$)	$\frac{\phi_1^2}{4}(r^{*2} - 1)$	—	—	—	—
2-Layer model ($N = 2$)	$C_4 \ln\frac{1}{\beta_2} + \frac{\phi_2^2}{4}(\beta_2^2 - 1)$	$C_4 \ln\frac{1}{r^*} + \frac{\phi_2^2}{4}(r^{*2} - 1)$	—	$\frac{\beta_2^2}{2}(\phi_2^2 - \chi_{1,2}\cdot\phi_1^2)$	—
3-Layer model ($N = 3$)	$C_5 \ln\frac{1}{\beta_3} + \frac{\phi_3^2}{4}(\beta_3^2 - 1) + C_4\left(\ln\frac{\beta_3}{\beta_2} + \frac{\phi_2^2}{4}(\beta_2^2 - \beta_3^2)\right) + \frac{\phi_1^2}{4}(r^{*2} - \beta_2^2)$	$C_5 \ln\frac{1}{\beta_3} + \frac{\phi_3^2}{4}(\beta_3^2 - 1) + C_4 \ln\frac{\beta_3}{r^*} + \frac{\phi_2^2}{4}(r^{*2} - \beta_3^2)$	$C_5 \ln\frac{1}{r^*} + \frac{\phi_3^2}{4}(r^{*2} - 1)$	$\frac{\beta_2^2}{2}(\phi_2^2 - \chi_{1,2}\cdot\phi_1^2)$	$\frac{\beta_3^2}{2}(\phi_3^2 - \chi_{2,3}\cdot\phi_2^2) + \frac{\beta_2^2}{2}(\chi_{2,3}\cdot\phi_2^2 - \chi_{1,3}\cdot\phi_1^2)$

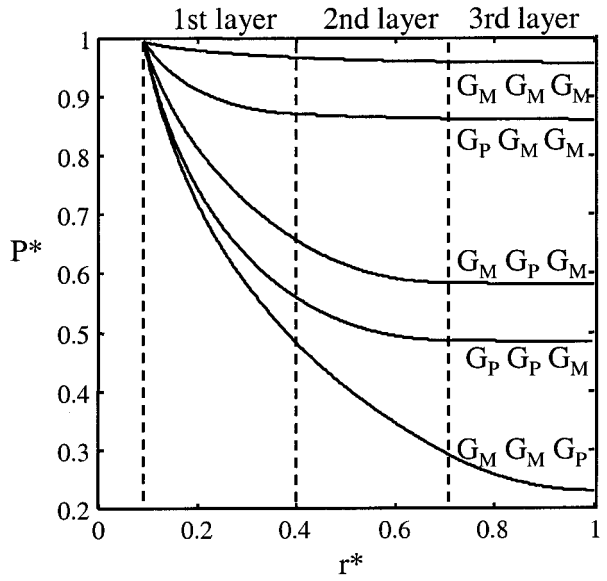

FIGURE 4 pO_2 profiles for the multilayer Kroghian model with granulocytic progenitors (G_P) and mature granulocytes (G_M). The cell types in the various combinations are listed with the first cell layer first, etc.

heterogeneities of cell type and cell location affect pO_2 distribution. G_M instead of G_P was chosen as the predominant cell type because hematopoietic cells or cell clusters with a larger ϕ value can be placed in the extravascular region without the occurrence of oxygen depletion. In reality, the BMHC may contain granulocytes of various stages of differentiation; however, we focused on mature granulocytes for computational simplicity. Tissue cylinders with 10 cell layers of G_M were simulated because it has been reported that as many as 20 hematopoietic cells can be found between two neighboring sinuses (Lichtman, 1984).

In our model, three different secondary cell types, megakaryocytes (Mk) (1 cell diameter, $\phi_2 = 0.396$); erythrocytes (E) (~8 cell diameters, $\phi_2 = 1.846$); and adipocytes (Ad) (1 cell diameter, $\phi_2 = 0.047$), were considered. These cells were placed near the sinus or near the boundary of the tissue cylinder occupied solely by mature granulocytes ($\phi_1 = 0.652$) (Figs. 5–7). The thickness of the extravascular tissue is 175 μm and the sinus radius is 5 μm, giving 0.0278 as β_1 and a corresponding ϕ_{max} of 0.805 for homogeneous tissue. The homogeneous tissue cylinder filled with G_M was used as a reference case for comparison (*dotted line*). The presence of a megakaryocyte ($\delta = 0.528$, $\phi_2 = 0.396$) near the rim of the tissue cylinder causes a slight asymmetry of pO_2 profiles, with pO_2 levels in the vicinity of the megakaryocyte higher than those in regions diametrically opposite to it (Fig. 5 *A*). The oxygen tensions at the rim of the tissue cylinder (P^*_{R2}) at points *A* and *B* are 0.37 and 0.39, respectively, which are fairly similar to those of the homogeneous mature granulocytic tissue ($P^*_{R2} = 0.35$ for both positions) (Table 3). The location of the megakaryo-

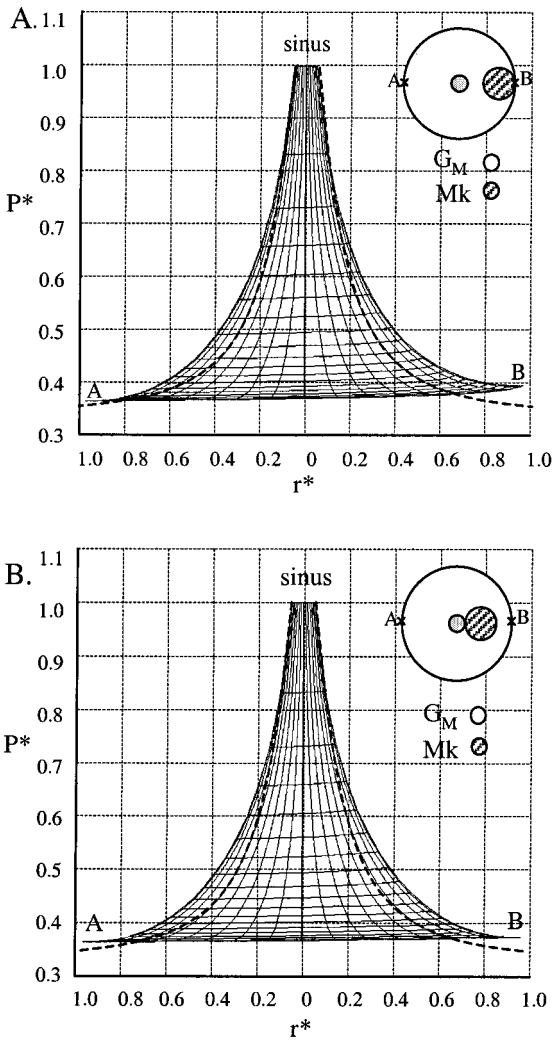

FIGURE 5 pO_2 profiles for two-dimensional Kroghian models at the far (*A*, $\xi = 0.736$) and close (*B*, $\xi = 0.292$) positions for mature granulocytes (G_M) as the predominant cell type and a megakaryocyte (Mk) as the secondary cell type ($R_1 = 5$ μm, $R_2 = 180$ μm, $\beta_1 = 0.0278$, $\beta_2 = 1$, $\phi_1 = 0.652$, $\phi_2 = 0.396$, $\delta = 0.528$).

TABLE 3 Oxygen tensions at the rim (P^*_{R2}) of tissue cylinders occupied by mature granulocytes and other hematopoietic cell types ($R_1 = 5$ μm and $R_2 = 180$ μm)

	Far Position*		Close Position*	
Secondary cell type	Point A	Point B	Point A	Point B
Megakaryocytes	0.37	0.39	0.37	0.37
Erythrocytes	0.33	0.24	0.33	0.31
Adipocytes†	0.44	0.58	0.44	0.58
Granulocytes‡	0.35	0.35	0.35	0.35

*The secondary cell type is located either far away from the sinus (far position) or next to the sinus (close position).
†Note that the close and far positions are equivalent due to the large size of an adipocyte.
‡No secondary cell type.

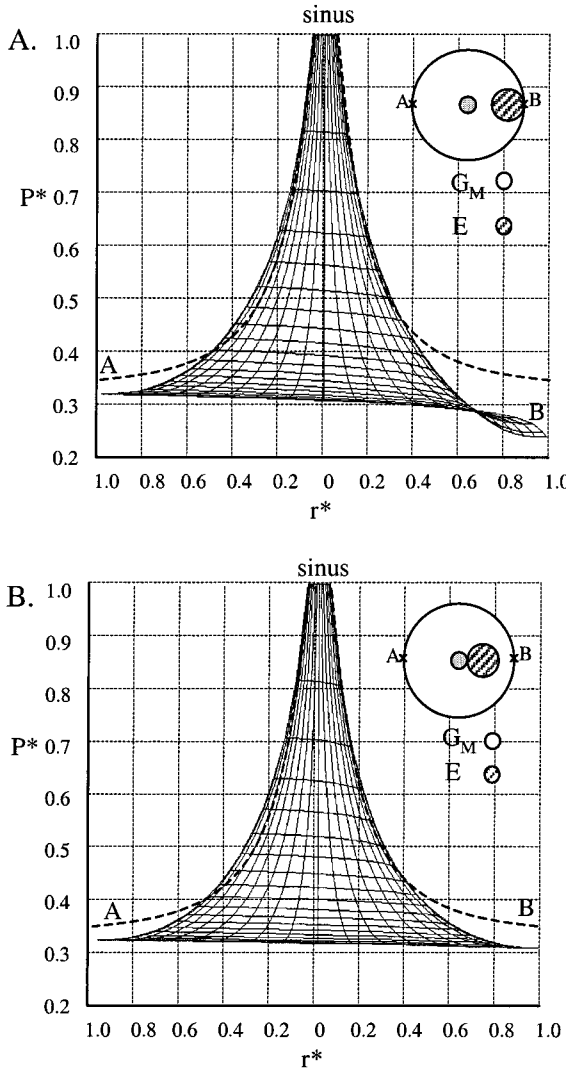

FIGURE 6 pO_2 profiles for two-dimensional Kroghian models at the far (*A*, $\xi = 0.819$) and close (*B*, $\xi = 0.208$) positions for mature granulocytes (G_M) as the predominant cell type and erythrocytes (E) as the secondary cell type ($R_1 = 5\ \mu m$, $R_2 = 180\ \mu m$, $\beta_1 = 0.0278$, $\beta_2 = 1$, $\phi_1 = 0.652$, $\phi_2 = 1.846$, $\delta = 0.361$).

cyte relative to the sinus has a minimal influence on the pO_2 distribution (Fig. 5 *B*). The presence of an erythroid cluster ($\delta = 0.361$, $\phi_2 = 1.846$) results in a steeper pO_2 gradient in its proximity, especially when it is away from a sinus (Fig. 6 *A*). Oxygen tensions are slightly lower than the reference case and pO_2 profiles become more symmetric when the erythroid cluster is placed next to the sinus (Fig. 6 *B* and Table 3). pO_2 distributions of hematopoietic tissue containing mature granulocytes and an adipocyte ($\delta = 0.972$, $\phi_2 = 0.047$) are highly asymmetric (Fig. 7). The P^*_{R2} values at points *A* and *B* for this cellular architecture differ by 34% (Table 3). Oxygen tensions are much higher than the reference case and pO_2 gradients progressively increase in the angular direction from the adipocyte (Fig. 7).

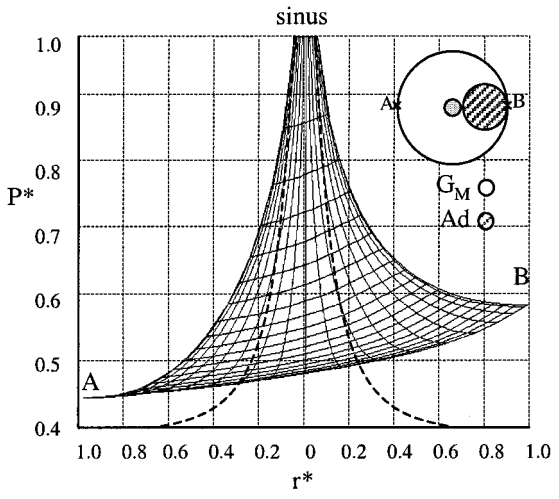

FIGURE 7 pO_2 profiles for two-dimensional Kroghian models for mature granulocytes (G_M) as the predominant cell type and an adipocyte (Ad) as the secondary cell type ($R_1 = 5\ \mu m$, $R_2 = 180\ \mu m$, $\beta_1 = 0.0278$, $\beta_2 = 1$, $\phi_1 = 0.652$, $\phi_2 = 0.047$, $\delta = 0.972$, $\xi = 0.486$).

pO_2 distribution in colony-type cellular arrangements

Using the equations shown in Table 2 and model parameters described in the companion paper (Chow et al., 2001), the pO_2 distribution in an erythroblastic islet (a macrophage surrounded by two layers of erythroid progenitors and four layers of mature erythrocytes) is shown as in Fig. 8. Hema-

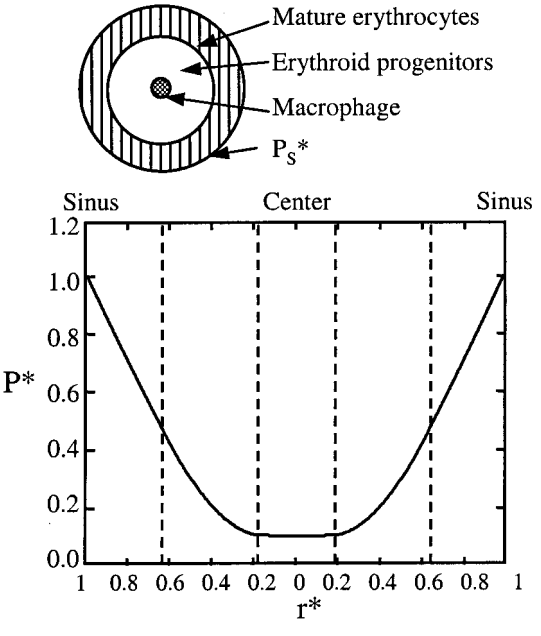

FIGURE 8 pO_2 profile for an erythroblastic islet in the multilayer Kroghian model with modified boundary conditions ($R_4 = 80\ \mu m$, $\beta_2 = 0.194$, $\beta_3 = 0.632$, $\beta_4 = 1$, $\phi_1 = 0.666$, $\phi_2 = 2.23$, $\phi_3 = 1.51$, $\chi_{1,2} = 2.01$, $\chi_{1,3} = 2.01$, $\chi_{2,3} = 1$).

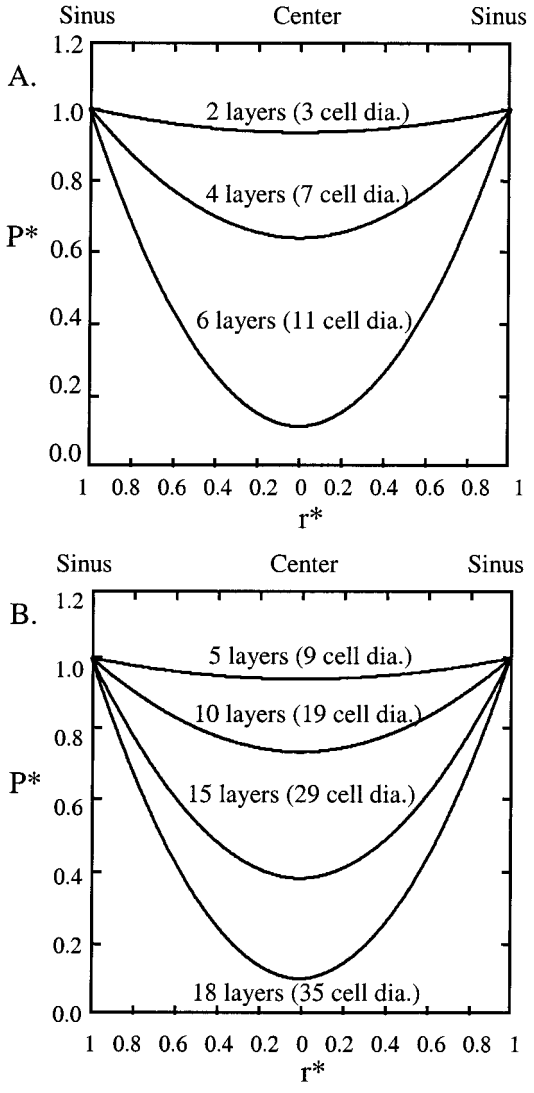

FIGURE 9 pO_2 profiles for (*A*) granulocytic loci and (*B*) lymphocytic nodules in the multilayer Kroghian model with modified boundary conditions (ϕ_1 values for granulocytic loci of 3, 7, and 11 cell diameters are 0.516, 1.20, and 1.89, respectively; ϕ_1 values for lymphocytic nodules of 9, 19, 29, and 35 cell diameters are 0.488, 1.03, 1.57, and 1.90, respectively).

topoietic cells at the outermost cell layer of the tissue cylinder experience the steepest pO_2 gradient, while variations in oxygen availability at the center of the tissue cylinder are minimal. Among all cells present in the erythroblastic islet, the macrophage experiences the lowest pO_2. Even though the size of tissue region considered (160 μm or 13 cell layers in diameter) is substantially larger than those simulated in the multilayer model, oxygen depletion does not occur due to the abundant oxygen supply from the surrounding vasculature.

Oxygen tension distributions in granulocytic loci (Fig. 9 A) and lymphocytic nodules (Fig. 9 B) of different diameters were estimated using a similar model formulation with only one cell type. The simulation results show that pO_2 at the center of the tissue cylinder drops substantially with an increasing number of cell layers. Simulated pO_2 distributions in the lymphocytic nodules (using the maximum reported q_{O2} value for all lymphocytes) indicated that oxygen limitation does not occur even for the lymphocytic nodule of a considerable size (35 cell diameters) (this is consistent with the fact that lymphocytic nodules of a diameter ranging from 80 to 1200 μm can be found in the BMHC). However, granulocytic progenitors in the granulocytic locus experience oxygen depletion when they are only 6–7 cell diameters away from the sinus.

DISCUSSION

Effects of heterogeneity in cellular properties and variation in cell location

Because the hematopoietic extravascular tissue is heterogeneous and complex in nature, we used more sophisticated models to examine how the coexistence of cells with different cellular properties affects oxygen availability. To minimize the number of cellular architectures considered, we focused on a simple model framework with granulocytes in which increasing layers of granulocytic progenitors were placed near the sinus or close to the rim of the tissue cylinder, and examined changes in pO_2 distributions in the multilayer Kroghian model (Fig. 4). Because cellular properties of a particular region in the tissue cylinder can strongly influence the overall pattern of pO_2 profiles, the pO_2 level and gradient experienced by individual cells are interrelated and strongly depend on characteristics of other cells present in the BMHC. Simulation results show that the position of a cell layer is also crucial in determining the pattern of pO_2 profiles because the tissue volume occupied by a cell layer next to the sinus is considerably smaller than the volume occupied by a cell layer farther away from the sinus. Thus, oxygen demand by cells in the outer region of a tissue cylinder affects the pO_2 distribution more than oxygen utilization by cells in the inner region.

Effects of cylindrical asymmetry on pO_2 distribution

In general, pO_2 profiles in the two-dimensional model are characterized by their asymmetry and localized variations in pO_2 distribution. The simulation results also indicate the importance of diffusion in the angular direction relative to the secondary cell type. The degree of asymmetry in the pO_2 distribution depends on the difference between ϕ_1 and ϕ_2. The presence of erythrocytes in the tissue cylinder occupied by mature granulocytes is associated with a localized reduction in pO_2 levels because ϕ_2 (erythrocytes) is about three times higher than ϕ_1 (mature granulocytes) (Fig. 6). However, a megakaryocyte or an adipocyte with a lower ϕ_2

value causes an increase in oxygen availability in its proximity (Figs. 5 and 7). In particular, substantial changes in pO_2 levels result from the difference in ϕ values of the adipocyte and mature granulocytes (ϕ_2 is ~14 times lower than ϕ_1). In addition, differences in the size of the secondary cell or cell cluster (δ) and its location (ξ) also contribute to variations in the pO_2 distribution. The total oxygen consumption of the secondary cell type correlates with the size of the cell cluster (Chow, 2000), and the location of the secondary cell type strongly affects the localized changes in pO_2 gradients (Fig. 6).

Physiological implications

Granulocytic progenitors will most likely experience low pO_2 even three to four cell diameters away from a sinus (Fig. 4) (six to seven cell diameters for granulocytic loci in a well-vascularized region (Fig. 9 *A*)). This is consistent with the findings that low pO_2 (in contrast to higher pO_2) promotes the expansion of both granulocytic progenitors and more differentiated granulocytes (Hevehan et al., 2000; Smith and Broxmeyer, 1986). The simulated results described in Fig. 4 represent a typical pO_2 distribution of a composite tissue, whereby the metabolically active cells located farther away from the sinus (rather than near the sinus) would cause lower pO_2 levels in their proximity. Not only can this simulated result be applied to granulocytic progenitors, but it can also be generalized for any progenitor cell type (erythrocytes and megakaryocytes). This agrees with the finding that low pO_2 promotes the expansion of hematopoietic progenitor cells such as burst-forming-unit erythroids (BFU-E; Koller et al., 1992; Rich and Kubanek, 1982), colony-forming-unit granulocyte-macrophages (CFU-GM; Hevehan et al., 2000, LaIuppa et al., 1998), and colony-forming-unit megakaryocytes (CFU-Mk; LaIuppa et al., 1998).

Our simulated results shown in Fig. 8 are also consistent with the physiology of an erythroblastic islet. The large (12–50 μm) macrophage at the center of the islet is a metabolically very active cell (Rich, 1986), which experiences the lowest pO_2 in the islet. It has been shown that low pO_2 enhances erythropoietin (Epo) production by macrophages, which are a source of extrarenal Epo (Rich, 1988). The macrophage is surrounded by primitive erythrocytes, which is consistent with our findings that low pO_2 promotes maintenance and expansion of erythroid progenitors (BFU-E) (Koller et al., 1992). The mature erythrocytes are located at the outer periphery of the islet and against the sinus wall, which is the area with the highest pO_2 values of the islet. This is also consistent with our findings that higher pO_2 promotes erythroid differentiation (La Iuppa et al., 1998).

Although the reasons why hematopoietic cells in the BMHC arrange in such an organized fashion remain unclear, we speculate that stem cells are located at the region with very low pO_2 levels (almost anoxic) because this prevents oxygen radicals from damaging these important cells, which are at a limited supply (unlike more differentiated cells) and probably have limited self-renewal capability. Also, the presence of oxygen is likely to induce cell cycling (assuming the presence of other nutrients and cytokines), while most stem cells are non-cycling. Therefore, more differentiated hematopoietic cells are most likely to be found near the sinus.

Model formulation

The original Kroghian model is not able to fully describe cellular architectures, in which multiple cell types exist in a cylindrically symmetric or non-symmetric manner. Other researchers have investigated a variety of alternatives to the Kroghian model to account for non-idealized geometry (Bailey, 1967; Piiper, 1992) and more complex capillary arrangements (Caligara and Rooth, 1961; Grunewald, 1973; Metzger, 1969, 1973; Secomb et al., 1992). We proposed a multilayer Kroghian model to examine tissue cylinders with concentric rings of mature granulocytes and granulocytic progenitors around the sinus. This model provided us with a simplified picture of the pO_2 distribution in a heterogeneous cell-type situation, which can serve as a reference for comparison to a two-dimensional model. In addition, simulation results can be used to eliminate cellular architectures that are physiologically unrealistic (for example, extensive oxygen depletion), thus minimizing the number of cases that must be considered in the two-dimensional Kroghian model.

BM microphotographs show that most cellular arrangements are not cylindrically symmetric. Thus, the two-dimensional Kroghian model is a logical extension of the multilayer heterogeneous model. It allowed us to explore more complex cellular architectures, which more closely mimic physiological cellular arrangements, in terms of the number of cells and their locations. It is interesting to note that deviations from the profiles of the homogeneous Kroghian model are less significant in the two-dimensional model than in the multilayer model. Finally, to simulate cellular architectures whereby cells grow in colony-like structures (erythroblastic islets, granulocytic loci, and lymphocytic nodules), we used a modified cylinder model without a sinus in the center but rather surrounded by sinuses on the outer periphery. In conclusion, not only does this study provide an insight into how the model formulation affects predicted oxygen availability in the extravascular hematopoietic tissue, but it also serves as a paradigm for mathematically estimating pO_2 distribution in tissues with multiple cell types and non-uniform cellular architectures.

APPENDIX

In the finite difference method (FDM), the mass transfer equation applying to element (i, j) (Eqs. 16 and 17) can be approximated with finite differences defined as

$$\frac{\partial P^*}{\partial r^*} \approx \frac{P^*_{i,j+1} - P^*_{i,j-1}}{2\Delta r^*} \tag{A1}$$

$$\frac{\partial^2 P^*}{\partial r^{*2}} \approx \frac{P^*_{i,j+1} + P^*_{i,j-1} - 2P^*_{i,j}}{\Delta r^{*2}} \tag{A2}$$

$$\frac{\partial^2 P^*}{\partial \theta^2} \approx \frac{P^*_{i-1,j} + P^*_{i+1,j} - 2P^*_{i,j}}{\Delta \theta^2} \tag{A3}$$

We thus obtain the following equation:

$$\frac{P^*_{i,j+1} + P^*_{i,j-1} - 2P^*_{i,j}}{\Delta r^{*2}} + \frac{1}{r^*_{i,j}} \frac{P^*_{i,j+1} - P^*_{i,j-1}}{2\Delta r^*} + \frac{1}{r^{*2}_{i,j}} \frac{P^*_{i-1,j} + P^*_{i+1,j} - 2P^*_{i,j}}{\Delta \theta^2} = \phi^2_{i,j} \tag{A4}$$

which can be rewritten in terms of constants $a_{i,j}$, $b_{i,j}$, $c_{i,j}$, and $d_{i,j}$.

$$a_{i,j}P^*_{i,j+1} + b_{i,j}P^*_{i,j-1} + c_{i,j}(P^*_{i-1,j} + P^*_{i+1,j}) - P^*_{i,j} = d_{i,j} \tag{A5}$$

$$a_{i,j} = \frac{\left[\left(\frac{r^*_{i,j}}{\Delta r^*}\right)^2 + \frac{r^*_{i,j}}{2\Delta r^*}\right]}{2\left[\left(\frac{r^*_{i,j}}{\Delta r^*}\right)^2 + \frac{1}{\Delta \theta^2}\right]} \tag{A6}$$

$$b_{i,j} = \frac{\left[\left(\frac{r^*_{i,j}}{\Delta r^*}\right)^2 - \frac{r^*_{i,j}}{2\Delta r^*}\right]}{2\left[\left(\frac{r^*_{i,j}}{\Delta r^*}\right)^2 + \frac{1}{\Delta \theta^2}\right]} \tag{A7}$$

$$c_{i,j} = \frac{\frac{1}{\Delta \theta^2}}{2\left[\left(\frac{r^*_{i,j}}{\Delta r^*}\right)^2 + \frac{1}{\Delta \theta^2}\right]} \tag{A8}$$

$$d_{i,j} = \frac{\phi^2_{i,j} \cdot r^{*2}_{i,j}}{2\left[\left(\frac{r^*_{i,j}}{\Delta r^*}\right)^2 + \frac{1}{\Delta \theta^2}\right]} \tag{A9}$$

We can write a similar equation for all the elements on the tissue cylinder in the two-dimensional Kroghian model, except those on the boundaries (Fig. 2). A system of algebraic equations (similar to Eq. A5 with different coefficients) relating oxygen tensions of different elements ($N_{tot} = M \times N$) is generated. The boundary conditions (Eqs. 18 and 19) can be rewritten to obtain equations relating oxygen tensions of those elements on the boundaries.

$$P^*_{i,1} = 1 \quad \text{for} \quad i = 1, \ldots, M$$

$$\text{(at the sinus wall)} \tag{A10}$$

$$\frac{P_{i,N}{}^* - P_{i,N-2}{}^*}{2\Delta r^*} = 0 \quad \text{fori} = 1, \ldots, M$$

$$\text{(at the rim of the tissue cylinder)} \tag{A11}$$

The boundary value problem (Eqs. A5, A10, and A11) can be written as

$$AX = B \tag{A12}$$

where A is an (N_{tot} by N_{tot}) matrix containing coefficients on the left-hand side of Eq. A5 and the boundary conditions, B, is an (N_{tot} by 1) matrix containing coefficients on the right-hand side of Eq. A5 and the boundary conditions, and X is an (N_{tot} by 1) matrix containing all the oxygen tensions on the mesh. Oxygen tension of each element is calculated using the least-squares method in the MATLAB software package (MathWorks, Natick, MA).

This work was supported by National Institutes of Health Grant R01HL48276.

REFERENCES

Adler, S. S. 1984. Blood circulation of bone marrow. *In* Blood Vessels and Lymphatics in Organ Systems. D. E. Abramson and R. B. Dobrin, editors. Academic Press, San Diego. 705–719.

Bailey, H. 1967. Oxygen exchange between capillary and tissue: some equations describing countercurrent and nonlinear transport. *In* Physical Bases of Circulatory Transport: Regulation and Exchange. E. Keeve and A. Guyton, editors. Saunders, Philadelphia. 353–366.

Caligara, F., and G. Rooth. 1961. Measurements of the oxygen diffusion coefficient in the subcutis of man. *Acta Physiol. Scand.* 53:114–127.

Chow, D. C. Modelling oxygen distribution in the hematopoietic compartment of bone marrow. M.S. thesis, Northwestern University, 2000.

Chow, D. C., L. A. Wenning, W. M. Miller, and E. T. Papoutsakis. 2001. Modeling pO_2 distributions in the bone marrow hematopoietic compartment. I. Krogh's model. *Biophys. J.* 81:675–684.

Collins, P. C., L. K. Nielsen, S. D. Patel, E. T. Papoutsakis, and W. M. Miller. 1998. Characterization of hematopoietic cell expansion, oxygen uptake, and glycolysis in a controlled, stirred-tank bioreactor system. *Biotechnol. Prog.* 14:466–472.

Federspiel, W. J. 1986. A model study of intracellular oxygen gradients in a myoglobin-containing skeletal muscle fiber. *Biophys. J.* 49:857–868.

Federspiel, W. J., and A. S. Popel. 1986. A theoretical analysis of the effect of the particulate nature of blood on oxygen release in capillaries. *Microvasc. Res.* 32:164–189.

Fletcher, J. E. 1978. Mathematical modeling of the microcirculation. *Math. Biosci.* 38:159–202.

Fletcher, J. E. 1980. On facilitated oxygen diffusion in muscle tissues. *Biophys. J.* 29:437–458.

Grossmann, U. 1982. Simulation of combined transfer of oxygen and heat through the skin using a capillary loop model. *Math. Biosci.* 61:205–236.

Grunewald, W. 1973. The influence of the three-dimensional capillary pattern on the intercapillary oxygen diffusion—a new composite model for comparison of calculated and measured oxygen distribution. *In* Oxygen Supply. M. Kessler, D. F. Bruley, L. C. Clark, Jr., D. W. Lubbers, I. A. Silver, and J. Strauss, editors. Urban & Schwarzenberg, Munchen-Berlin-Wien. 5–17.

Hevehan, D. L., E. T. Papoutsakis, and W. M. Miller. 2000. Physiologically significant effects of pH and oxygen tension in granulopoiesis. *Exp. Hematol.* 28:267–275.

Hoofd, L., C. Bos, and Z. Turek. 1994. Modeling erythrocytes as point-like O_2 sources in a Kroghian cylinder model. *Adv. Exp. Med. Biol.* 345: 893–900.

Hoofd, L., and F. Kreuzer. 1979. A new mathematical approach for solving carrier-facilitated steady-state diffusion problems. *J. Math. Biol.* 8:1–13.

Hoofd, L., Z. Turek, and K. Rakusan. 1987. Diffusion pathways in oxygen supply of cardiac muscle. *Adv. Exp. Med. Biol.* 215:171–177.

Ivanov, K. P., Y. Y. Kislyakov, and M. O. Samoilov. 1979. Microcirculation and transport of oxygen to neurons of the brain. *Microvasc. Res.* 18:434–441.

Koller, M. R., J. G. Bender, W. M. Miller, and E. T. Papoutsakis. 1992. Reduced oxygen tension increases hematopoiesis in long-term culture of human stem and progenitor cells from cord blood and bone marrow. *Exp. Hematol.* 20:264–270.

LaIuppa, J. A., E. T. Papoutsakis, and W. M. Miller. 1998. Oxygen tension alters the effects of cytokines on the megakaryocyte, erythrocyte, and granulocyte lineages. *Exp. Hematol.* 26:835–843.

Lichtman, M. A. 1984. The relationship of stromal cells to hematopoietic cells in marrow. *In* Long-Term Bone Marrow Culture, 1st Ed. D. G. Wright and J. S. Greenberger, editors. Alan R. Liss Inc., New York. 3–29.

Metzger, H. 1969. Distribution of oxygen partial pressure in a two-dimensional tissue supplied by capillary meshes and concurrent and countercurrent systems. *Math. Biosci.* 5:143–154.

Metzger, H. 1973. Geometric considerations in modeling oxygen transport processes in tissue. *In* Oxygen Transport to Tissue, Pharmacology, Mathematical Studies, and Neonatology. D. Bruley and H. Bicher, editors. Plenum Press, New York. 761–772.

Na, T. Y. 1979. Computational Methods in Engineering Boundary Value Problems. Academic Press Inc., New York.

Piiper, J. 1992. Oxygen supply by perfusion and diffusion in heterogeneous tissue models. *In* Oxygen Transport to Tissue XIV. W. Erdmann and D. F. Bruley, editors. Plenum Press, New York.

Popel, A. S. 1982. Oxygen diffusive shunts under conditions of heterogeneous oxygen delivery. *J. Theor. Biol.* 96:533–541.

Popel, A. S., C. K. Charny, and A. S. Dvinsky. 1986. Effects of heterogeneous oxygen delivery on the oxygen distribution in skeletal muscle. *Math. Biosci.* 81:91–114.

Rakusan, K., L. Hoofd, and Z. Turek. 1984. The effect of cell size and capillary spacing on myocardial oxygen supply. *Adv. Exp. Med. Biol.* 180:463–475.

Reneau, D. D., Jr., D. F. Bruley, and M. H. Knisely. 1967. A mathematical simulation of oxygen release, diffusion, and consumption in the capillaries and tissue of the human brain. *In* Chemical Engineering in Medicine and Biology. D. Hershey, editor. Plenum Press, New York. 135.

Rich, I. N. 1986. A role of the macrophage in normal hemopoiesis. II. Effect of varying physiological oxygen tensions on the release of hemopoietic growth factors from bone marrow-derived macrophage in vitro. *Exp. Hematol.* 14:746–751.

Rich, I. N. 1988. The macrophage as a production site for hematopoietic regulator molecules: sensing and responding to normal and physiological signals. *Anticancer Res.* 8:1015–1040.

Rich, I. N., and B. Kubanek. 1982. The effect of reduced oxygen tension on colony formation of erythropoietic cells in vitro. *Br. J. Haematol.* 52:579–588.

Secomb, T. W., R. Hsu, and M. W. Dewhirst. 1992. Models for oxygen exchange between microvascular networks and surrounding tissue. *Advances in Biological Heat and Mass Transfer (ASME).* 231:121–127.

Smith, S., and H. E. Broxmeyer. 1986. The influence of oxygen tension on the long-term growth in vitro of hematopoietic progenitor cells from human cord blood. *Br. J. Haematol.* 63:29–34.

Tavassoli, M. J., and M. Yoffey. 1983. Bone marrow: structure and function. Alan R. Liss Inc., New York.

Weiss, L. P. 1991. Functional organization of the hematopoietic tissues. *In* Hematology—Basic Principles and Practice, 8th Ed. R. Hoffman, E. J. Benz, S. J. Shattil, B. Furie, and H. J. Cohen, editors. Churchill Livingstone, New York. 82–86.

Wickramasinghe, S. N. 1975. Human Bone Marrow. Blackwell Scientific Publications, Oxford, distributed by J. B. Lippincott, Philadelphia.